COMPUTING SPECULAR POINTS OVER COMPLEX LAND SURFACES FOR AIRBORNE GNSS-R APPLICATIONS

Xiaoyou Lin[1], Delwyn Moller[1], Andrew O'Brien[2], Ryan Linnabary[3], Chris Ruf[4]

1) Dept. of Electrical, Computer and Software Engineering, University of Auckland, New Zealand
2) ElectroScience Laboratory, The Ohio State University, Columbus, OH USA
3) University Corporation for Atmospheric Research (UCAR), Boulder, CO USA
4) Dept. of Electrical Engineering and Computer Science, University of Michigan, MI, USA

ABSTRACT

This paper proposes a novel global-to-local (G2L) searching algorithm to find the locations of specular reflections over terrestrial surfaces for GNSS-R applications. In the proposed method, an initial coordinate of the specular reflection is first computed on a smooth WGS84 datum using the Fibonacci method. Second, a local coordinate frame that is centered at the initial WGS84 specular point (SP) is defined with respect to the local topography, and the G2L searching algorithm is applied to more precisely locate the specular reflection point. The effects of the complex land topography, including the local slope and incidence angles, are considered. This method is simulated for an airborne GNSS-R scenario where the receiver position is based on historical flight data from Gisborne to Wellington in New Zealand, where the results show that the finalized SP positions have been significantly shifted due to the complex topographical surfaces. This G2L method can be implemented to accurately track the location of reflected GNSS signal power from measured delay-Doppler maps (DDM) for land applications.

Index Terms— Bistatic radar, CYGNSS, GNSS-R, Rongowai, specular point

1. INTRODUCTION

Global Navigation Satellite System Reflectometry (GNSS-R) leverages the bistatic reflections of signals transmitted from GNSS constellations (e.g., GPS, Galileo and GLONASS) to perform earth remote sensing. This technique has been successfully employed in a variety of applications including ocean altimetry, retrieval of ocean surface wind speeds, and monitoring the soil moisture [1]. GNSS-R has been proven to work in a number of space-based missions (e.g, [2]). However, GNSS-R instruments on aircraft can also offer observations with improved spatial resolution and quality to complement and further inform spaceborne GNSS-R

retrievals, especially in more complex terrestrial scattering scenarios [3].

In a unique partnership, New Zealand and the USA are developing the Rongowai mission [4] whereby a next-generation GNSS-R receiver (NGRx) developed at the University of Michigan for NASA's Earth Science Technology Office [5] will be integrated onto an Air New Zealand domestic Q300 aircraft. Scheduled for installation in mid-2022, this permanent airborne GNSS-R instrument will enable unique and comprehensive science collections over many years and over a wide variety of land surfaces for further analysis for the science community. For terrestrial surfaces, determining the location of the GNSS reflection is complicated by topography, and a first step is to determine the position where these reflected signals are coming from.

It is well known that the greatest contribution of the scattered signal power at the receiver comes from the region at and around the specular point (SP), which for simple surfaces is the location that minimizes the propagation path and satisfies Snell's law between incidence and scattering angles [6], [7]. However, unlike scattering from ocean, computing the electromagnetic scattering from the land surfaces possesses more challenges because of several factors, such as inhomogeneous scenes and mixed coherent/incoherent scattering [4].

The Rongowai mission will have extensive and dense measurement coverage over widely varying terrain that will require an efficient method for geolocating the reflections. Thus, this paper proposes a global-to-local (G2L) algorithm to search for the locations of specular reflections over complex land surfaces by considering the local slope and facing angles. The proposed algorithm is validated using simulations of flight from Gisborne to Wellington in New Zealand, where the results show that significant shifts can be observed between the finalized and initial SPs.

2. GLOBAL-TO-LOCAL SEARCHING ALGORITHM

As presented in Fig. 1(a), the overall G2L searching algorithm consists of two steps. With the help of Fibonacci se-
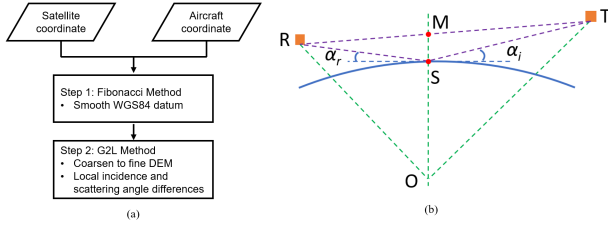
Fig. 1. G2L algorithm to compute the location of specular point: (a) flowchart, and (b) geometrical relationship.

quence, the first step computes the initial positions of specular reflections made by specific satellite and aircraft positions when assuming a smooth WGS84 earth datum. Consequently, the second step proposes the G2L algorithm by defining a "global" area centered at the initial SP. In this global area, the incidence (θ_i) and scattering angles (θ_s) are computed over a coarsened digital elevation map (DEM), where the facet with minimal difference between θ_i and θ_s is selected. Then, we zoom in at the selected facet to render the DEM at a higher resolution to perform the searching algorithm again. This step ends after a few iterations when the DEM search resolution is at a comparable size to the Fresnel zone, which is defined as the "local" area. The coordinates of the facet at the final iteration is regarded as the position of the SP.

2.1. Step 1: Fibonacci Method

As illustrated in Fig. 1(b), there exist three requirements that a specular reflection should satisfy: 1) on the arc segment $\overset{\frown}{ab}$; 2) equal incidence and reflection angle (i.e., $\alpha_i = \alpha_r$); and 3) minimal distance from the satellite to the SP to the receiver.

One approach to find the position of SP is to gradually narrow the searching domain in accordance with the principle of the shortest path. One popular algorithm in this category is the golden-section search (GSS) method [8]. However, in this step, we will utilize Fibonacci sequence to compute the initial location of SP. Compared to the GSS method, Fibonacci method defines the searching domain that can converge to the desired range of acceptance in a faster manner.

The flowchart of Step 1 is illustrated in Fig. 2. Here, the start and end points of the searching domain are defined by:

$$\begin{cases} \lambda_k = a_k + \frac{F_{n-k-1}}{F_{n-k+1}}(b_k - a_k), \\ \mu_k = a_k + \frac{F_{n-k}}{F_{n-k+1}}(b_k - a_k), \end{cases} \quad (1)$$

where $k = 1, 2, ..., n-1$, $a_1 = \vec{R}$ and $b_1 = \vec{T}$ are the coordinates of the receiver and transmitter in the earth-centered earth-fixed (ECEF) coordinate frame, respectively. Besides, F_k is the Fibonacci sequence, which follows

$$F_k = \frac{1}{\sqrt{5}} \left\{ \left(\frac{1+\sqrt{5}}{2}\right)^{k+1} - \left(\frac{1-\sqrt{5}}{2}\right)^{k+1} \right\}. \quad (2)$$
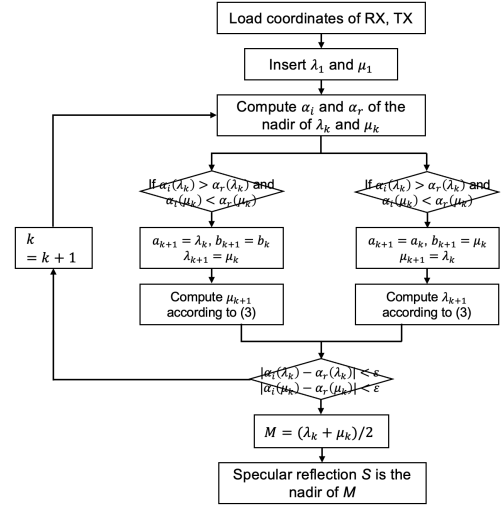

Fig. 2. Flowchart of Step 1 to compute initial specular points.

In each iteration, the α_i and α_r of the nadir of λ_k or μ_k is compared to determine the parameters that needs to be updated in the $(k+1)$th iteration. The iteration ends when $|\alpha_i - \alpha_r|$ is smaller than a predefined threshold ε.

It is worth noting that, unlike the existing works, Step 1 computes the α_i and α_r rather than the path distance $\vec{TS}$ and $\vec{SR}$. This is because for airborne applications, $\vec{SR}$ is negligible compared to $\vec{TS}$, which may lead to errors when computing the SP.

2.2. Step 2: G2L Algorithm

Definitely, the incidence and scattering angles (θ_i and θ_s) are not always the same if the initial SP determined by Step 1 is located on land. Thus, Step 2, the G2L algorithm computes the precise location of SP by considering the local incidence and scattering angles, denoted by θ_{li} and θ_{ls}, respectively.
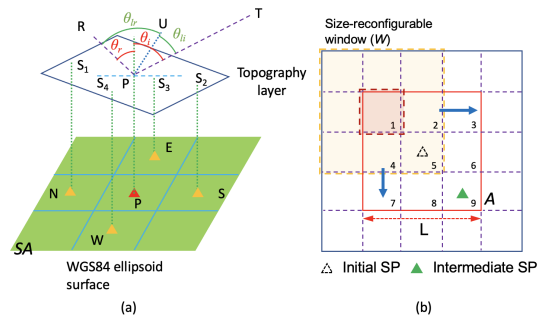
Fig. 3. (a) Compute local θ_i and θ_i, and (b) "global" to "local" computation of each grid in the candidate area.

To compute θ_{li} and θ_{ls} of an arbitrary point (P), we will start from considering a squared area (SA) centered at P. As illustrated in Fig. 3(a), assume the four points S_1, S_2, S_3 and

1861

S_4 that denote the local north, south, east and west of SA, respectively. Thus, the unit vectors of local east, north and up of SA can be defined by:

$$\hat{e} = \frac{\vec{S_3} - \vec{S_4}}{|S_3 - S_4|}, \tag{3}$$

$$\hat{n} = \frac{\vec{S_1} - \vec{S_2}}{|S_1 - S_2|}, \tag{4}$$

$$\hat{u} = \hat{e} \times \hat{n}. \tag{5}$$

Subsequently, θ_{li} and θ_{ls} can be computed from:

$$\theta_{li} = \mathrm{acos}\left(\frac{\overrightarrow{TS} \cdot (-\hat{u})}{\overrightarrow{TS}}\right), \tag{6}$$

$$\theta_{ls} = \mathrm{acos}\left(\frac{\hat{u} \cdot \overrightarrow{SR}}{\overrightarrow{SR}}\right). \tag{7}$$

Second, we apply (3)–(7) to successively compute the incidence and scattering angles from the "global" to the "local" area through a number of iterations. As illustrated in Fig. 3(b), assume the area A (red square) centered at the initial SP (dashed triangle) has the side length of L and has been divided into a 3×3 grids labelled from 1 to 9, where L is determined by the area illuminated by the antenna. This area A is defined as the "global" area. Besides, we also define a size-reconfigurable window (W), regarded as the SA defined in the above step, to slide within A to compute θ_{li} and θ_{ls} of each grid in A.

After obtaining the θ_{li} and θ_{ls} of all the grids, the grid with minimal difference between θ_{li} and θ_{ls} is defined to have the intermediate SP (e.g., the solid green triangle in the grid labelled as 9). Thus, this grid is selected to be zoomed in and further divided into a 3×3 grid matrix. Note that when applying the W, its side length also need to be adjusted to suit the size of the subgrid in this iteration. Subsequently, the θ_{li} and θ_{ls} of each subgrid in this subarea are computed to select the one with minimal angle difference. The above process repeats until the size of the subgrid meets the desired resolution, which is determined by the size of the Fresnel zone, and this subgrid is defined as the "local" area. The total number of iterations N can be computed from: $N = \log_3(L/l)$, where l is the desired resolution of the final iteration. Note that (L/l) is the number of grids along one side of A. However, we should include 1 more extra grid at each side of A in the computation to derive θ_{li} and θ_{ls} at the boundary of A.

Subsequently, the grid with the minimal angle difference at the last iteration is the location of the SP.

3. NUMERICAL RESULTS

In this section, we will implement the proposed G2L algorithm to simulate the SPs for a historical flight from Gisborne to Wellington in New Zealand on January 1, 2019, where the land types over the flight path include low-relief, ocean and mountain areas. The flight path retrieved from Opensky Network is plotted by the white dashed line in Fig. 4. Although the NGRx is capable of simultaneously receiving on 20 channels, we assessed just one satellite in this simulation, GPS BIIRM-1 (PRN 17).

Using the Fibonacci Method, Step 1 computes the initial SPs along the flight path as illustrated by the yellow dots in Fig. 4. The GSS method has also been used in Step 1, where we found that the total iterations is around 17% more than using the Fibonacci method.
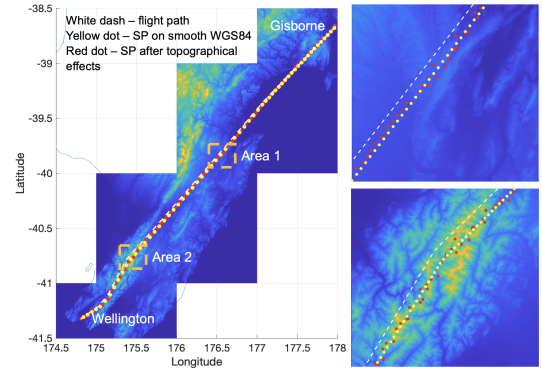
**Fig. 4**. Computed initial and finalized SPs for a historical Q300 flight.

For step 2 and the G2L search it is necessary to determine the spatial resolution of the final "local" iteration. We determine this by calculating the semi-major axis of the Fresnel zone as follows:

$$a = \frac{\sqrt{\lambda H_R \cos\theta}}{\cos^2\theta}, \tag{8}$$

where λ is the wavelength, H_R is the height of the aircraft above the ground, and θ is the incidence angle. In this particular case, $a \approx 36\,\mathrm{m}$, which is approximately the resolution of the 1-arc second DEM generated by the Shuttle Radar Topography Mission ($30\,\mathrm{m}$).

Here, we will demonstrate a step-by-step process of Step 2 to compute the finalized SP with one specific position of the aircraft of this historical flight. In this example, the ECEF coordinates of the satellite and aircraft are $T = (-1.628, 0.262, -2.015) \times 10^7\,\mathrm{m}$ and $R = (-0.496, 0.210, -3.991) \times 10^7\,\mathrm{m}$, respectively, whereas the computed latitude, longitude and altitude (LLA) coordinate of the corresponding SP is $(-38.9775°, 177.5714°, 0\,\mathrm{m})$. The side length L of the global area A is chosen to be $2430\,\mathrm{m}$, and hence, the total number of iterations is computed to be $N = \log_3(2430/30) = 4$.

As illustrated in Fig. 5, the initial SP (dashed triangle) is centered at the region whose raw resolution is $30\,\mathrm{m}$. Then, following Fig. 3(b), the resolution of A is coarsened

1862
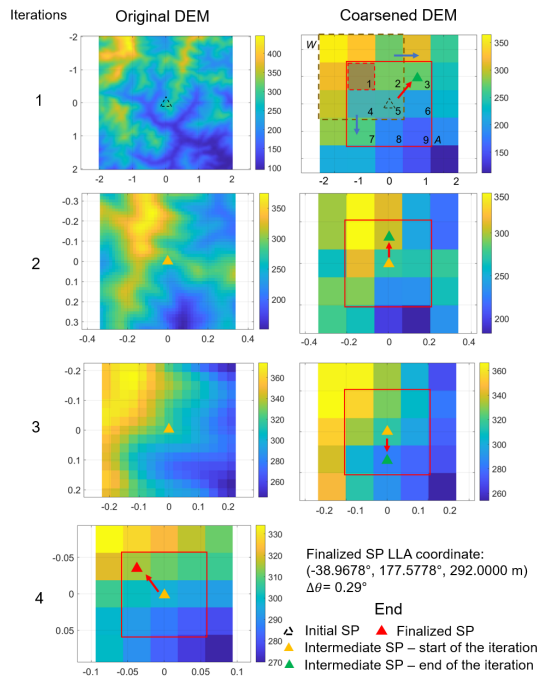
Fig. 5. Illustration of Step 2, where x and y axes are in kilometers, and the colorbar is the elevation in meters.

to $90\,\mathrm{m}$ (3×3 average), and a size-reconfigurable window (W) is defined. Finally, (3)–(7) are applied to determine the intermediate SP (green triangle in the $3\mathrm{rd}$ grid) in this iteration by finding the minimal angle difference between θ_{li} and θ_{ls}. The second iteration zooms in the $3\mathrm{rd}$ grid in the first iteration and repeats the above process. After four iterations, the LLA coordinate of the finalized SP is $(-38.9678°, 177.5778°, 292.0\,\mathrm{m})$, and the difference between θ_{li} and θ_{ls} at this finalized position is $0.29°$. It has to be clarified that there can exist multiple SPs for rough topography, we will further optimize this with the ongoing mission. Nevertheless, this example illustrates a mathematical approximation that tends to produce a reasonable result.

The finalized SPs along the flight path are plotted by the red dots in Fig. 4. Fig. 4 also zooms in the flight path, initial and finalized SPs for two areas. Area 1 is a relatively flat area where the initial and finalized SPs are almost the same. Area 2 is a mountainous area and the varying topography significantly affects the locations of the SP. We intend to implement and validate this algorithm for operational geolocation of the NgRx reflections for the Rongowai mission.

4. CONCLUSION AND FUTURE WORK

This paper presents a novel G2L method to simulate the position of specular reflections for GNSS-R applications over terrestrial surfaces on a routine basis. This method consists of two steps, the first step computes the initial SP on a bare-Earth WGS84 datum. The second step then defines a "global" area around the initial SP and iteratively searches for the location where the angle difference between incidence and scattering angles is minimised at the resolution of the Fresnel zone. We demonstrated our method for a representative historical flight from Gisborne to Wellington in New Zealand illustrating the impact of topography for locating the specular reflections.

To extend this work, first, we will validate this G2L method by using the DDMs generated by the NGRx during the science flights. Second, coherent and incoherent reflection coefficients due to complex surfaces will be analyzed based on the positions of SP found by this method.

5. REFERENCES

[1] S. Gleason, S. Hodgart, Y. Sun, C. Gommenginger, S. Mackin, and et al., "Detection and processing of bistatically reflected gps signals from low earth orbit for the purpose of ocean remote sensing," *IEEE Trans. Geosci. Remote Sens.*, vol. 43, no. 6, pp. 1229–1241, 2005.

[2] C. Ruf, M. Unwin, J. Dickinson, R. Rose, D. Rose, and et al., "Cygnss: Enabling the future of hurricane prediction," *IEEE Geosci. Remote Sens. Mag.*, vol. 1, no. 2, pp. 52–67, 2013.

[3] A. Perez-Portero, J. F. Munoz-Martin, H. Park, and A. Camps, "Airborne gnss-r: A key enabling technology for environmental monitoring," *IEEE J. Sel. Topics Appl. Earth Observ. Remote Sens.*, vol. 14, pp. 6652–6661, 2021.

[4] D. Moller, C. Ruf, R. Linnabary, A. O'Brien, and S. Musko, "Operational airborne gnss-r aboard air new zealand domestic aircraft," in *2021 IEEE Int. Geosci. Remote Sens. Symp.*, 2021, pp. 1284–1287.

[5] C. Ruf, R. Backhus, T. Butler, C. Chen, S. Gleason, and et al., "Next generation gnss-r instrument," in *2020 IEEE Int. Geosci. Remote Sens. Symp.*, 2020, pp. 3353–3356.

[6] L. King, M. Unwin, J. Rawlinson, R. Guida, and C. Underwood, "Towards a topographically-accurate reflection point prediction algorithm for operational spaceborne gnss reflectometry—development and verification," *Remote Sensing*, vol. 13, no. 5, pp. 1031, 2021.

[7] A. Camps, "Spatial resolution in gnss-r under coherent scattering," *IEEE Geosci. Remote Sens. Lett.*, vol. 17, no. 1, pp. 32–36, 2020.

[8] J. Mashburn, P. Axelrad, S. T. Lowe, and K. M. Larson, "An assessment of the precision and accuracy of altimetry retrievals for a monterey bay gnss-r experiment," *IEEE J. Sel. Topics Appli. Earth Observ. and Remote Sens.*, vol. 9, no. 10, pp. 4660–4668, 2016.